

## Modeling wave generation by borehole orbital vibrator source

Seiji Nakagawa<sup>1</sup> and Thomas M. Daley<sup>1</sup>

### ABSTRACT

An orbital vibrator source (OVS), a fluid-coupled shear-wave source, has many properties useful for cross-well, single-well, and borehole-to-surface imaging of both P- (compressional) and S- (shear) wave velocities of reservoir rocks. To this day, however, only a limited number of quantitative models have been developed to explain its properties. In this article, we develop both 2D and 3D models of an OVS, allowing us to examine source characteristics such as radiation patterns, frequency dependence of wave amplitudes, and guided-wave generation. These models are developed in the frequency-wavenumber domain using the partial wave expansion of the wavefield within and outside the borehole. The models predict many unique characteristics of an OVS, including formation-property-dependent vibrator amplitudes, uniform isotropic S-wave radiation pattern, and small tube-wave generation.

### INTRODUCTION

The orbital vibrator source (OVS) was originally developed by Conoco in the 1980s to generate S-waves from a fluid-filled borehole without the direct mechanical coupling of borehole seismic sources to the borehole wall [see Cole (1997) for a summary of the background of the orbital source]. There are two types of borehole OVS: a mechanical source (Figure 1a) and a solid-state, piezoelectric source (Figure 1b). Currently, only the mechanical source is used for field applications, so we will primarily discuss its wave-generation mechanism.

The mechanical source consists of an eccentric mass spinning around the source axis, encased in a cylindrical housing suspended in the borehole fluid. The centrifugal force induced by the rotation of the mass moves the whole source in the radial directions of the borehole, compressing the fluid on one side of the source and introducing tension on the other side

(Figure 2). On the borehole wall, these pressure perturbations generate shear motions that are, in principle, both vertically (parallel to the borehole, SV) and horizontally (perpendicular to the borehole, SH) polarized. Because of this wave-generating mechanism, the resulting waves have the same primary frequency as the spin frequency of the source. Current mechanical sources can generate waves with useful amplitudes at frequencies between approximately 70 and 400 Hz. The same wave-generating effect can be produced using a phased, circular array of piezoelectric sources around the borehole axis, generating waves above 4 kHz (e.g., Cole, 1997).

An OVS has many unique and attractive properties as a fluid-coupled, borehole S-wave source. For example, unlike conventional borehole sources that generate SV-waves (e.g., Van Schaack et al., 1995), the orbital source generates SH-waves with large amplitudes for a wide range of vertical (borehole-parallel) source-receiver offsets. Also, an OVS tends to generate only small tube waves (borehole-guided waves primarily supported by the compressional motion of the borehole fluid) that contaminate body waves used for seismic imaging (e.g., Cole, 1997). Furthermore, the source allows efficient decomposition of SH-waves and the other wave components through the superposition of phase-delayed, circularly polarized wave motions in both clockwise and counterclockwise directions around the borehole (Daley and Cox, 2001).

Although many successful applications of the borehole OVS have been reported, (Liu et al., 1991; Hardage, 1992; Liu et al., 2000), the mechanism of wave generation and the characteristics of waves generated by an OVS are not fully understood. A quantitative model is still needed to predict source characteristics such as radiation pattern and tube-wave generation and for applications such as anisotropy measurements and waveguide characterization of surrounding formations. Among several attempts to model the OVS (e.g., Daley and Cox, 2001; Novascone et al., 2002; Reynolds and Cole, 2002), Dong (1994a, b) and Dong et al. (1995) develop an analytical source model as input to a boundary element model. In this approach, the rotary motion of the vibrator is modeled as a rotating radial force applied to the borehole wall,

Presented in part at the 73rd Annual Meeting, Society of Exploration Geophysicists. Manuscript received by the Editor June 28, 2004; revised manuscript received April 10, 2005; published online January 12, 2006.

<sup>1</sup>E. O. Lawrence Berkeley National Laboratory, Center for Computational Seismology (CCS), Earth Sciences Division, Berkeley, California 94720. E-mail: snakagawa@lbl.gov; tmdaley@lbl.gov.

© 2006 Society of Exploration Geophysicists. All rights reserved.

which is subsequently integrated over angular and depth directions of the borehole. The basic principle of Dong's model is also used in our study to model the 3D wavefield generated by the OVS and is extended to examine the amplitudes of the generated waves as a function of physical source parameters and possible generation of higher-order mode waves and borehole-guided waves.

In this paper, we introduce analytical models to examine the waves generated by an OVS. A 2D model is first introduced that takes into account the mechanical interaction between a rigid source body with specified physical parameters and the surrounding borehole fluid and rock. Subsequently, a 3D source model is proposed that is conceptually similar

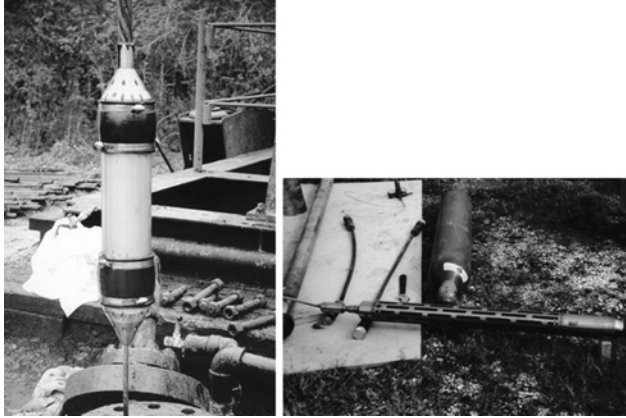


Figure 1. Borehole OVSs. Currently, only the mechanical OVS (left) is used in the field. The piezoelectric OVS (right) generates waves by sequentially firing an array of piezoelectric elements and potentially can generate waves at much higher frequencies.

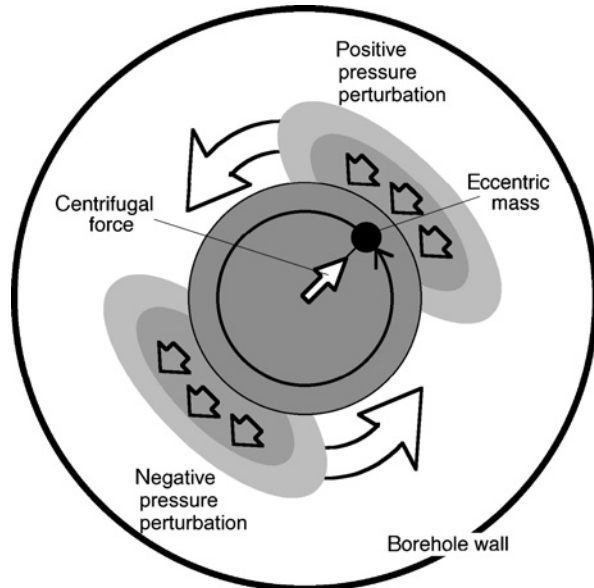


Figure 2. A cross section of a mechanical OVS within a borehole. The rotational motion of the source induced by a spinning eccentric mass generates rotating positive and negative pressure perturbations within the fluid.

to the model used by Kurkjian and Chang (1986) to examine the waves generated by stationary (nonrotating) multipole sources. The initially unknown source amplitude is determined using the 2D model. These models have an advantage over fully numerical models based on finite-difference methods and boundary-element methods because they allow us to analyze the relationship between OVS motions and borehole-guided waves, including tube waves. Using the introduced model, we examine the radiation pattern of body waves generated by an OVS and the characteristics of cogenerated borehole-guided waves.

## MODELING METHODS

In this section we derive both 2D and 3D OVS models based upon series expansion of the wavefield via cylindrical waves.

### Two-dimensional representation of an OVS

To determine the relationship between the wavefield generated by an OVS and physical source parameters, we first examine a 2D model, assuming an infinitely long, circular, rigid source along the borehole with a radius  $r_0$  and a mass per unit length  $M_s$  (including an eccentric mass  $M_e$  at a radius  $r_e$ ) within a fluid-filled circular borehole with a radius  $a$ . Also, the rock surrounding the borehole is assumed to be isotropic and homogeneous. Although such a generalization can be made easily, we do not assume a casing wall or mud-cake layers on the fluid-rock interface. The 2D model described here is similar to the model derived by Reynolds and Cole (2002), who examine the pressure within the borehole fluid and the power radiated by the OVS into the surrounding rock.

An OVS is driven by a centrifugal force  $\mathbf{F}_e$  resulting from a spinning eccentric mass within the source that is counteracted by the sum of fluid pressure  $\mathbf{F}_p$  and the inertial force of the source. For stationary source motions with a circular frequency  $\omega$ , this force equilibrium is written as

$$\mathbf{F}_e + \mathbf{F}_p = -(M_s - M_e)\omega^2 \mathbf{U}, \quad (1)$$

where  $\mathbf{U}$  is the rigid body displacement of the source. In the following derivations, we assume that the magnitude of the centrifugal force is always given by  $M_e r_e' \omega^2$ , where  $r_e' = r_e(M_s - M_e)/M_s$  is the radius of rotation for the eccentric mass around the center of the mass. Since the rotation results in a  $\pi/2$  phase shift between the two orthogonal components of the force and displacement, using complex notations and Cartesian coordinates the first term in equation 1 can be computed by

$$\mathbf{F}_e = \begin{bmatrix} F_{ex} \\ F_{ey} \end{bmatrix} = M_e r_e' \omega^2 \begin{bmatrix} 1 \\ i \end{bmatrix} e^{-i\omega t}. \quad (2)$$

The source displacement is given by

$$\mathbf{U} = \begin{bmatrix} U_x \\ U_y \end{bmatrix} = U_0 \begin{bmatrix} 1 \\ i \end{bmatrix} e^{-i\omega t}. \quad (3)$$

We need to determine the amplitude and phase of  $U_0$ . This is done by applying a set of boundary conditions on the source-fluid boundary and the fluid-rock boundary.

To obtain an explicit form of solutions for the wavefield around the source, we assume that the particle motions

induced by the source are small (less than 1 mm) and the source frequency is sufficiently low (below megahertz). As shown in Appendix A, under these assumptions, the displacement and stress field around the source are acoustic, and the wavefield can be expressed by a superposition of cylindrical waves (Appendix B). The assumption for small amplitudes can be validated afterward by using the source displacement amplitude obtained in this section with the acoustic approximation.

First, since the radial component of the source displacement  $U_r$  and the fluid displacement  $u_r$  must be continuous on the source-fluid boundary at  $r = r_0$ ,

$$\begin{aligned} u_r(r = r_0) &= U_0(\cos \phi + i \sin \phi)e^{-i\omega t} = U_0 e^{i(\phi - \omega t)} \\ &= \sum_{n=-\infty}^{\infty} \left[ A_n^{P+} \partial_r H_n^{(1)}(k_{P1}r_0) + A_n^{P-} \partial_r H_n^{(2)}(k_{P1}r_0) \right] \\ &\quad \times e^{i(n\phi - \omega t)} \\ \therefore U_0 &= A_1^{P+} \partial_r H_1^{(1)}(k_{P1}r_0) + A_1^{P-} \partial_r H_1^{(2)}(k_{P1}r_0), \end{aligned} \quad (4)$$

where  $\partial_r$  indicates partial derivative of the function via the radial variable  $r$ . Definitions for the unknown expansion coefficients are given in Appendix B. This boundary condition leads to a requirement that all terms  $n \neq 1$  be identically zero. This forces both the displacement and pressure field around the OVS to be given by the first-order Bessel functions in the radial direction and by the first harmonic component in the angular direction. The latter characteristic indicates that OVS can be viewed as a rotating dipole source that generates rotating distribution of positive and negative pressure perturbations within the fluid on the opposite sides of the circular body (Figure 2)

Next, the total force from the fluid pressure perturbation  $p$  surrounding the source is computed by

$$\begin{aligned} \mathbf{F}_p &= \int_0^{2\pi} (-p) \begin{bmatrix} \cos \phi \\ \sin \phi \end{bmatrix} r_0 d\phi \\ &= -\rho_1 \omega^2 \int_0^{2\pi} \Phi_p^{(s)} \begin{bmatrix} \cos \phi \\ \sin \phi \end{bmatrix} r_0 d\phi \\ &= -\rho_1 \omega^2 \left[ A_1^{P+}(\omega) H_1^{(1)}(k_{P1}r_0) \right. \\ &\quad \left. + A_1^{P-}(\omega) H_1^{(2)}(k_{P1}r_0) \right] \int_0^{2\pi} e^{i(\phi - \omega t)} \begin{bmatrix} \cos \phi \\ \sin \phi \end{bmatrix} r_0 d\phi, \\ &= -\pi r_0 \rho_1 \omega^2 \left[ A_1^{P+}(\omega) H_1^{(1)}(k_{P1}r_0) \right. \\ &\quad \left. + A_1^{P-}(\omega) H_1^{(2)}(k_{P1}r_0) \right] \begin{bmatrix} 1 \\ i \end{bmatrix} e^{-i\omega t} \end{aligned} \quad (5)$$

where the relationship

$$-p = \rho_1 c_{P1}^2 \nabla^2 \Phi_p^{(s)} = -\rho_1 \omega^2 \Phi_p^{(s)} \quad (6)$$

is used for the 2D P-wave Helmholtz potential  $\Phi_p^{(s)}$  for the source. From the force equilibrium in equation 1, using equations 2 and 5,

$$\begin{aligned} M_e r_e - \pi r_0 \rho_1 \left[ A_1^{P+} H_1^{(1)}(k_{P1}r_0) + A_1^{P-} H_1^{(2)}(k_{P1}r_0) \right] \\ = -(M_s - M_e) U_0, \end{aligned} \quad (7)$$

where the common term  $\omega^2 [1 \ i]^T e^{-i\omega t}$  is suppressed ( $T$  indicates the vector or matrix transposition). On the fluid-rock boundary at  $r = a$ , the radial component of both displacement and stress (pressure)  $\sigma_{rr}$  is continuous, and the tangential (shear) component of stress  $\sigma_{r\phi}$  vanishes. These conditions are

$$\begin{aligned} u_r(r = a) &= \partial_r H_1^{(1)}(k_{P1}a) A_1^{P+} + \partial_r H_1^{(2)}(k_{P1}a) A_1^{P-} \\ &= \partial_r H_1^{(1)}(k_{P2}a) B_1^P + (i/a) H_1^{(1)}(k_{S2}a) B_1^S, \end{aligned} \quad (8)$$

$$\begin{aligned} \sigma_{rr}(r = a) &= -\rho_1 \omega^2 \left[ H_1^{(1)}(k_{P1}a) A_1^{P+} + H_1^{(2)}(k_{P1}a) A_1^{P-} \right] \\ &= \rho_2 c_{S2}^2 \left[ -(2D_r + k_{S2}^2) B_1^P H_1^{(1)}(k_{P2}a) \right. \\ &\quad \left. + 2i D_r B_1^{SH} H_1^{(1)}(k_{S2}a) \right], \end{aligned} \quad (9)$$

$$\begin{aligned} \sigma_{r\phi}(r = a) &= 0 \\ &= \rho_2 c_{S2}^2 \left[ 2i D_r B_1^P H_1^{(1)}(k_{P2}a) \right. \\ &\quad \left. + (2D_r + k_{S2}^2) B_1^{SH} H_1^{(1)}(k_{S2}a) \right], \end{aligned} \quad (10)$$

where we introduce an operator

$$D_r \equiv \frac{1}{r} \frac{\partial}{\partial r} - \frac{1}{r^2} = \frac{\partial}{\partial r} \frac{1}{r}. \quad (11)$$

The dependence on  $e^{i(\phi - \omega t)}$  of all the terms in equations 8–11 is understood and omitted. The five boundary conditions are combined to obtain a linear system of equations:

$$\begin{bmatrix} -\frac{M_e - M_e}{\pi r_0^2} & H_1^{(1)}(k_{P1}r_0) & H_1^{(2)}(k_{P1}r_0) & 0 & 0 \\ -1 & \partial_r H_1^{(1)}(k_{P1}r_0) & \partial_r H_1^{(2)}(k_{P1}r_0) & 0 & 0 \\ 0 & -\partial_r H_1^{(1)}(k_{P1}a) & -\partial_r H_1^{(2)}(k_{P1}a) & \partial_r H_1^{(1)}(k_{P2}a) & (i/a) H_1^{(1)}(k_{S2}a) \\ 0 & -\rho_1 \omega^2 H_1^{(1)}(k_{P1}a) & -\rho_1 \omega^2 H_1^{(2)}(k_{P1}a) & \rho_2 c_{S2}^2 (2D_r + k_{S2}^2) H_1^{(1)}(k_{P2}a) & -2i \rho_2 c_{S2}^2 D_r H_1^{(1)}(k_{S2}a) \\ 0 & 0 & 0 & 2i D_r H_1^{(1)}(k_{P2}a) & (2D_r + k_{S2}^2) H_1^{(1)}(k_{S2}a) \end{bmatrix} \times \begin{bmatrix} U_0 \\ A_1^{P+} \\ A_1^{P-} \\ B_1^P \\ B_1^{SH} \end{bmatrix} = \begin{bmatrix} \frac{M_e}{\pi r_0^2} r_e \\ 0 \\ 0 \\ 0 \\ 0 \end{bmatrix} \quad (12)$$

Equation 12 can easily be solved analytically. The solution for  $U_0$  can be expressed as

$$U_0 = \left( -\frac{M_e}{M_s} r_e \right) \times \frac{1}{1 - \frac{\pi r_0 \rho_1}{M_s - M_e} \frac{d_1}{d_2}}, \quad (13)$$

where

$$\begin{bmatrix} d_1 \\ d_2 \end{bmatrix} \equiv \mathbf{H}_{r_0} (\mathbf{H}_a)^{-1} \begin{bmatrix} c_1 \\ c_2 \end{bmatrix}, \quad (14)$$

$$\mathbf{H}_a \equiv \begin{bmatrix} H_1^{(1)}(k_{P1}a) & H_1^{(2)}(k_{P1}a) \\ \partial_r H_1^{(1)}(k_{P1}a) & \partial_r H_1^{(2)}(k_{P1}a) \end{bmatrix}, \quad (15)$$

$$\mathbf{H}_{r_0} \equiv \begin{bmatrix} H_1^{(1)}(k_{P1}r_0) & H_1^{(2)}(k_{P1}r_0) \\ \partial_r H_1^{(1)}(k_{P1}r_0) & \partial_r H_1^{(2)}(k_{P1}r_0) \end{bmatrix}, \quad (16)$$

$$\begin{bmatrix} c_1 \\ c_2 \end{bmatrix} \equiv \begin{bmatrix} \frac{\rho_2}{\rho_1 k_{S2}^2} \left( 2D_r + k_{S2}^2 \right) H_1^{(1)}(k_{P2}a) - \frac{\rho_2}{\rho_1 k_{S2}^2} 2i D_r H_1^{(1)}(k_{S2}a) \\ \partial_r H_1^{(1)}(k_{P2}a) \quad \frac{i}{a} H_1^{(1)}(k_{S2}a) \end{bmatrix} \times \begin{bmatrix} (2D_r + k_{S2}^2) H_1^{(1)}(k_{S2}a) \\ -2i D_r H_1^{(1)}(k_{P2}a) \end{bmatrix}. \quad (17)$$

The term within parentheses in equation 13 is the displacement of an OVS in vacuum (or air), modified by the following term containing rock and borehole fluid properties.

For the special case of an OVS within an infinite fluid, the coefficients for waves propagating toward the source  $A_1^{P-}$  and the waves within the rock  $B_1^P$  and  $B_1^{SH}$  can be set to zero. Therefore, equation 12 reduces to

$$\begin{bmatrix} -\frac{M_s - M_e}{\pi r_0 \rho_1} & H_1^{(1)}(k_{P1}r_0) \\ -1 & \partial_r H_1^{(1)}(k_{P1}r_0) \end{bmatrix} \begin{bmatrix} U_0^\infty \\ A_1^{P+} \end{bmatrix} = \begin{bmatrix} \frac{M_e}{\pi r_0 \rho_1} r'_e \\ 0 \end{bmatrix}, \quad (18)$$

which results in

$$U_0^\infty = \left( -\frac{M_e}{M_s} r'_e \right) \times \frac{1}{1 - \frac{\pi r_0 \rho_1}{M_s - M_e} \frac{H_1^{(1)}(k_{P1}r_0)}{\partial_r H_1^{(1)}(k_{P1}r_0)}} \quad (19)$$

and the source potential

$$\begin{aligned} \Phi_p^{(s)} &= A_1^{P+} H_1^{(1)}(k_{P1}r) e^{i(\phi - \omega t)} \\ &= \frac{U_0^\infty}{\partial_r H_1^{(1)}(k_{P1}r_0)} H_1^{(1)}(k_{P1}r) e^{i(\phi - \omega t)}. \end{aligned} \quad (20)$$

This result is used to determine the amplitude of a 3D OVS in the next section.

In Figure 3, the source displacement amplitude is shown as a function of frequency for sources within vacuum, infinite fluid,

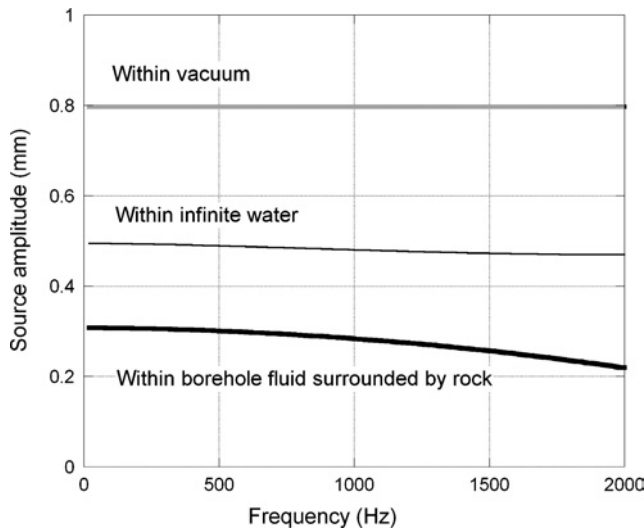


Figure 3. A comparison of source displacements for OVSs suspended within vacuum (air), infinite water, and a fluid-filled borehole surrounded by rock. The baseline source and material parameters are given in Table 1.

and borehole fluid surrounded by rock. The model parameters used in this example are shown in Table 1. The displacement amplitudes of the source for the frequencies of our interest (70 ~ 400 Hz) are nearly constant. Also, the amplitude of the sources within an infinite fluid and a finite-diameter borehole are reduced from a source within a vacuum as a result of the impedance effect of the surroundings.

### Three-dimensional representation of OVS

Unlike the 2D case, the 3D geometry of an OVS is difficult to model analytically. As an alternative, we represent the source by a circular array of phase-delayed point dilation (or volume displacement) sources located around the borehole axis. This representation of a borehole source is similar to Kurkjian and Chang's (1986) model used to examine waves generated by fluid-coupled, multipole borehole sources for well logging. Phase delays between the individual sources of Kurkjian and Chang's model are either zero or  $\pi$  radians. In contrast, phase delays within the point-source array for the OVS change continuously from zero to  $2\pi$  (counterclockwise spin) or zero to  $-2\pi$  (clockwise spin). Therefore, collectively, this source array does not change the net volume of the fluid within the borehole as seen for the physical, 2D source.

Using the partial-wave expansion technique, the radiation and scattering of the waves generated by an OVS can be examined analytically using the frequency-wavenumber integration technique and solved numerically by the discrete wavenumber method. A single time-harmonic volume source with a magnitude  $V_0(\omega)$ , located at the center of an infinite acoustic medium, generates a wavefield with a single scalar Helmholtz potential (e.g., Lee and Balch, 1982; Kurkjian and Chang, 1986) given by

$$\begin{aligned} & -\frac{V_0(\omega)}{4\pi R} e^{i\omega(R/c_{P1}-t)} \\ &= -\frac{i V_0(\omega)}{8\pi} \int_{-\infty}^{+\infty} H_0^{(1)}(k_r^{P1} r') e^{i(k_z z - \omega t)} dk_z, \end{aligned} \quad (21)$$

where  $R$  is the source-receiver distance,  $k_r^{P1} = \sqrt{(\omega/c_{P1})^2 - k_z^2}$  with  $k_z$  the  $z$ -direction (borehole-parallel) wavenumber, and  $r'$  is the projection of  $R$  onto the plane perpendicular to the  $z$ - or borehole axis. In expression 21,  $V_0$  has a dimension of [volume/length] for a single circular array of point sources (1D array) and [volume/length<sup>2</sup>] for circular arrays also distributed in the  $z$ -direction (2D array). Throughout the rest of this article, the positive and negative sign conventions are used for wavenumbers and frequencies, respectively, as in equation 21. Also, since wavenumber components are examined individually, the source potential term is

$$s_{V_0} = -\frac{i V_0(\omega)}{8\pi} H_0^{(1)}(k_r^{P1} r') e^{i(k_z z - \omega t)}. \quad (22)$$

We represent an OVS, located on the borehole axis and with a vibration frequency  $\omega$ , as a series of point-volume sources located at a radius  $r = r_0$  around the borehole axis (Figure 4). Each source, located at an angular coordinate  $\theta$  measured from the  $x$ -axis, has a phase delay  $\exp(i\theta)$ , resulting in a constant phase rotating around the borehole axis at a spin frequency  $\omega$ .

To compute the superimposed effect of the off-center point sources, we first examine the waves generated by a single point source at  $(r_0, \theta)$ . The origin of the coordinate in equation 22 is shifted along the  $x'$  axis by  $r_0$  (Figure 4b). This involves a coordinate transform via

$$r \cos(\phi - \theta) = r_0 + r' \cos \psi, \quad (23)$$

$$r \sin(\phi - \theta) = r' \sin \psi, \quad (24)$$

where  $r$  and  $\phi$  are the radial and angular coordinates of the receiver and where  $\psi$  is the angular coordinate of the receiver around the source, measured from the  $x'$  axis. Equations 23 and 24 imply

$$r' = \sqrt{r^2 + r_0^2 - 2rr_0 \cos(\phi - \theta)}. \quad (25)$$

Using equation 25, we express the potential given by a single Hankel function around the source via an infinite series of partial waves using the relationships

$$\begin{aligned} H_0^{(1)}(k_r^{P1} r') &= H_0^{(1)}(k_r^{P1} \sqrt{r^2 + r_0^2 - 2rr_0 \cos(\phi - \theta)}) \\ &= \sum_{n=-\infty}^{\infty} \left\{ \begin{array}{l} J_n(k_r^{P1} r_0) H_n^{(1)}(k_r^{P1} r) \text{ (if } r > r_0 \geq 0) \\ J_n(k_r^{P1} r) H_n^{(1)}(k_r^{P1} r_0) \text{ (if } r_0 > r \geq 0) \end{array} \right\} \\ &\quad \times \exp(in(\phi - \theta)). \end{aligned} \quad (26)$$

The overall effect of the phase-delayed sources (Figure 4c) is computed by introducing equation 26 into equation 22 and integrating the resulting expression with a phase-delay factor  $\exp(i\theta)$  over the values of the angle  $0 < \theta < 2\pi$ . For reasons that will become clear shortly, we generalize this delay factor as  $\exp(im\theta)$  ( $m = \dots, -2, -1, 0, 1, 2, \dots$ ). An OVS with these delay factors can be viewed as a generalized OVS with multiple cycles of pressure oscillation around the source. The angular integration with these delay factors involves the orthogonality relationship

$$\int_0^{2\pi} e^{in(\phi-\theta)} e^{im\theta} d\theta = 2\pi e^{in\phi} \delta_{m,n}, \quad (27)$$

where  $\delta_{m,n}$  is the Kronecker delta. With relationship 27, the source potential for a 1D array is given by

$$\begin{aligned} \Phi_p^{(s)}(z) &= \int_0^{2\pi} s_{V_0} e^{im\theta} r_0 d\theta \\ &= -\frac{i V_0(\omega)}{8\pi} r_0 e^{i(k_z z - \omega t)} \end{aligned}$$

**Table 1. Model parameters.**

Baseline material parameters			Source/borehole parameters		
Fluid density	$\rho_1$	1000 g/cm <sup>3</sup>	Source length	$L$	61.0 cm
Fluid P velocity	$c_{P1}$	1460 m/s	Source radius	$r_0$	5.08 cm
Rock density	$\rho_2$	2100 g/cm <sup>3</sup>	Source mass per length	$M_s$	14.9 kg/m
Rock P velocity	$c_{P2}$	3000 m/s	Eccentric mass radius	$r_e$	7.29 mm
Rock S velocity	$c_{S2}$	1731 m/s	Eccentric mass per length	$M_e$	1.62 kg/m
			Borehole diameter	$a$	7.62 cm

$$\begin{aligned} &\times \sum_{n=-\infty}^{\infty} \left\{ \begin{array}{l} J_n(k_r^{P1} r_0) H_n^{(1)}(k_r^{P1} r) \text{ (if } r > r_0 \geq 0) \\ J_n(k_r^{P1} r) H_n^{(1)}(k_r^{P1} r_0) \text{ (if } r_0 > r \geq 0) \end{array} \right\} \\ &\times \int_0^{2\pi} e^{in(\phi-\theta)} e^{im\theta} d\theta \\ &= -\frac{i V_0(\omega)}{4} r_0 \\ &\times \left\{ \begin{array}{l} J_m(k_r^{P1} r_0) H_m^{(1)}(k_r^{P1} r) \text{ (if } r > r_0 \geq 0) \\ J_m(k_r^{P1} r) H_m^{(1)}(k_r^{P1} r_0) \text{ (if } r_0 > r \geq 0) \end{array} \right\} \\ &\times e^{i(m\phi + k_z z - \omega t)}. \end{aligned} \quad (28)$$

An OVS with a finite length (i.e., 2D array) can be modeled by the superposition of the above sources distributed along the borehole axis (e.g., Dong, 1994a,b). For vibrator length  $L$ , equation 28 is integrated for sources distributed along the borehole axis, resulting in

$$\begin{aligned} \Phi_p^{(s)}(z; L) &= \int_{-L/2}^{+L/2} \Phi_p^{(1)}(z - \zeta) d\zeta \\ &= \Phi_p^{(s)}(z) \int_{-L/2}^{+L/2} \exp(-ik_z \zeta) d\zeta = \Phi_p^{(s)}(z) \\ &\quad \times \frac{2}{k_z} \sin\left(\frac{k_z L}{2}\right) = \Phi_p^{(s)}(z) L \text{sinc}\left(\frac{k_z L}{2}\right), \end{aligned} \quad (29)$$

which is the source potential for the 1D array modulated by a sinc (sampling) function. Note that the dimension of the source potential differs between the single array and the distributed array (finite-length source).

Equation 28 indicates that the phase delay among the point sources constituting an OVS selects a single term out of the infinite series of the partial-wave expansion. From equation 28, a ring-shaped expansion source (e.g., Dong et al., 1995) can be viewed as a generalized orbital source of the order  $m = 0$  and the currently used mechanical OVS of the order  $m = 1$ . Pressure distribution around the generalized OVSs is shown schematically in Figure 5. These sources can be viewed as the multipole sources used for S-wave borehole logging (Chen and Eriksen, 1991) that rotate around the borehole axis. Also note that the superposition of the two OVSs of the same order but with opposite spin directions results in

$$\begin{aligned} &\Phi_p^{(s)}(m) + \Phi_p^{(s)}(-m) \\ &= -\frac{i V_0(\omega)}{2} r_0 \left\{ \begin{array}{l} J_m(k_r^{P1} r_0) H_m^{(1)}(k_r^{P1} r) \text{ (if } r > r_0 \geq 0) \\ J_m(k_r^{P1} r) H_m^{(1)}(k_r^{P1} r_0) \text{ (if } r_0 > r \geq 0) \end{array} \right\} \\ &\quad \cos(m\phi) e^{i(k_z z - \omega t)}, \end{aligned} \quad (30)$$

which is the stationary (nonrotating) multipole source solution examined by Kurkjian and Chang (1986).

For the  $m = 1$  source, it is possible to relate self-consistently the point-volume source amplitude  $V_0(\omega)$  to the physical source parameters as we did for the 2D OVS. However, the source amplitude is not only a function of source parameters but is also dependent upon the borehole geometry and

material properties of the surrounding fluid and rock. As an approximation, we derive an expression of  $V_0(\omega)$  for the OVS in an infinite fluid as a function of source parameters and fluid properties. This is done by making the length of the source infinitely long and also integrating for all wavenumbers:

$$\begin{aligned}\Phi_{P,2D}^{(s)} &= \int_{-\infty}^{+\infty} \lim_{L \rightarrow \infty} \Phi_P^{(1)}(z; L) dk_z \\ &= \int_{-\infty}^{+\infty} \Phi_P^{(s)}(z) \lim_{L \rightarrow \infty} \frac{\sin(k_z L/2)}{k_z/2} dk_z \\ &= \int_{-\infty}^{+\infty} \Phi_P^{(s)}(z) 2\pi \delta(k_z) dk_z \\ &= -V_0(\omega) \frac{i\pi r_0}{2} J_1(k_{P1} r_0) H_1^{(1)}(k_{P1} r) e^{i(\phi - \omega t)}, \quad (31)\end{aligned}$$

where  $\delta(k_z)$  is the Dirac delta function. By comparing equations 31 and 20,

$$V_0(\omega) = \frac{2iU_0^\infty}{\pi r_0 J_1(k_{P1} r_0) \partial_r H_1^{(1)}(k_{P1} r_0)}, \quad (32)$$

where  $U_0^\infty$  is the complex source amplitude in equation 19 containing physical source parameters.

For 3D problems, the boundary conditions used to solve for the unknown coefficients  $A_n^P$ ,  $B_n^P$ ,  $B_n^{SH}$ , and  $B_n^{SV}$  in the series expansions of displacement in Appendix B are the continuity of radial displacement and normal stress (pressure) and two vanishing shear-stress components on the borehole wall. These four conditions can be applied to obtain a linear system of equations for the four coefficients for individual modes  $n$ . Note that an OVS of the order  $m$  can excite only the partial

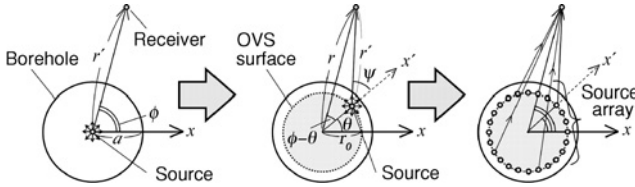


Figure 4. Representation of a 3D OVS using point volumetric sources. A single-point volume source (left) is first shifted to the radius of the OVS. Subsequently, the source potentials for these shifted point sources (center) are superimposed with a phase shift that changes continuously around the OVS.

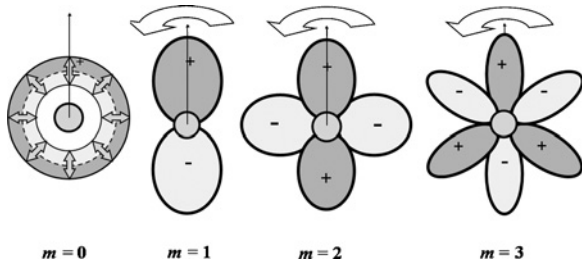


Figure 5. Distribution of fluid pressure perturbation around OVSs with different orders. Except for the zero-order source (monopole), these sources can be viewed as rotating multipole sources (order  $m$ ).

waves with  $n = m$ . The resulting linear system of equations is

$$\begin{bmatrix} -\partial_{P1} & \partial_{P2} & im & ik_z a \partial_{S2} \\ (1/\mu_2) \rho_1 \omega^2 a^2 & -(\lambda_2/\mu_2) k_{P2}^2 a^2 + 2\partial_{P2}^2 & 2im(-1 + \partial_{S2}) & 2ik_z a \partial_{S2}^2 \\ 0 & im(-2 + \partial_{P2}) + im\partial_{P2} & -\partial_{S2}^2 + \partial_{S2} - m^2 & -2mk_z a(-1 + \partial_{S2}) \\ 0 & 2ik_z a \partial_{P2} & -mk_z a & ((k_r^{S2} a)^2 - (k_z a)^2) \partial_{S2} \end{bmatrix} \times \begin{bmatrix} J_m(k_r^{P1} a) \\ H_m^{(1)}(k_r^{P2} a) \\ H_m^{(1)}(k_r^{S2} a) \\ H_m^{(1)}(k_r^{S2} a) \end{bmatrix} \times \begin{Bmatrix} A_m^P \\ B_m^P \\ B_m^{SH} \\ B_m^{SV} \end{Bmatrix} \equiv \mathbf{M}_m \begin{Bmatrix} A_m^P \\ B_m^P \\ B_m^{SH} \\ B_m^{SV} \end{Bmatrix} = \mathbf{s}_m, \quad (33)$$

where  $\mathbf{s}_m$  is the source term computed from equation 28 as

$$\mathbf{s}_m = -\frac{iV_0(\omega)}{4} r_0 J_m(k_r^{P1} r_0) \begin{Bmatrix} \partial_{P1} \\ -\rho_1 a^2 \omega^2 / \mu_2 \\ 0 \\ 0 \end{Bmatrix} H_m^{(1)}(k_r^{P1} a). \quad (34)$$

In equations 33 and 34, the symbols  $\partial_P$  and  $\partial_S$ , with subscript 1 denoting inside the borehole and subscript 2 denoting outside, are defined as

$$\partial_{P,S} Z_m \equiv (k_r^{P,S} a) \left. \frac{dZ_m(z)}{dz} \right|_{z=k_r^{P,S} a}, \quad (35)$$

where  $Z_m$  are Bessel functions of the appropriate kind. Also note that equations 21–23 are scaled by the borehole radius  $a$ . These equations can be constructed and solved for a given combination of wave frequency and  $z$ -direction wavenumber. The displacements are computed by introducing the resulting potentials into equations B-2, B-3, and B-4.

## EXAMPLES AND DISCUSSIONS

In this section we show several examples from the predictions made by the models developed in the preceding section.

### Comparison of 2D physical and fictitious OVS

We derive the 3D OVS model by imposing a radial outgoing wavefield within the borehole fluid (a fictitious source). However, this approach does not account for the interaction of the source and the waves reflected by the borehole wall, as would be the case for the true source shown in Figure 2. To estimate the error introduced by this approximation, we compare the waves generated by a physical source in the section “Two-Dimensional Representation of an OVS” and the waves generated by the fictitious source, which are computed by embedding the 2D outgoing wavefield from an OVS within an infinite fluid.

For the fictitious source, the wavefield within the borehole is given by a superposition of the source wavefield and the acoustic wavefield that is nonsingular at the center of the borehole, forcing the use of the Bessel function of the first kind.

The system equation to be solved is

$$\begin{bmatrix} -\partial_r J_1(k_{P1}a) & \partial_r H_1^{(1)}(k_{P2}a) & (i/a)H_1^{(1)}(k_{S2}a) \\ -\rho_1\omega^2 J_1(k_{P1}a) & \rho_2c_{S2}^2(2D_r + k_{S2}^2)H_1^{(1)}(k_{P2}a) & -2i\rho_2c_{S2}^2D_r H_1^{(1)}(k_{S2}a) \\ 0 & 2iD_r H_1^{(1)}(k_{P2}a) & (2D_r + k_{S2}^2)H_1^{(1)}(k_{S2}a) \end{bmatrix} \times \begin{bmatrix} A_1^P \\ B_1^P \\ B_1^{SH} \end{bmatrix} = \begin{bmatrix} \partial_r H_1^{(1)}(k_{P1}a) \\ \rho_1\omega^2 H_1^{(1)}(k_{P1}a) \\ 0 \end{bmatrix} \times \frac{U_0^\infty}{\partial_r H_1^{(1)}(k_{P1}a)}. \quad (36)$$

Comparing the solutions from equations 36 and 12, the accuracy of the approximation can be evaluated.

Figure 6 compares of P- and S-wave amplitudes in the rock at a receiver located 100 m away from the source. The model parameters are shown in Table 1. This example illustrates that the amplitude of the waves from using the fictitious source is 5% to 10% smaller than the physical source for up to several kilohertz.

**Driving-point impedance effect of a 2D OVS**

As we saw in Figure 3, the amplitude of the source motion is dependent on the physical properties of surrounding rocks. This indicates that the source motion of an OVS tool itself can be used for borehole logging of rock properties. This idea has been introduced and both theoretically and experimentally examined by Novascone et al. (2002), who term this the driving-point impedance effect.

Using the 2D OVS model in equation 13, we can perform a series of sensitivity studies for the rock properties (density, P- and S-wave velocities). Again, using the baseline properties in Table 1, the amplitudes of the source as a function of wave frequency and rock properties are shown in Figure 7. From Figure 7a we can see that the source motion is practically insensitive to the formation P-wave velocity for the frequencies of our interest (below a few kilohertz). In contrast, the source motion shows appreciable sensitivity to the density and S-wave velocity (Figures 7b and 7c). However, the sensitivity generally is very small for frequencies below the current

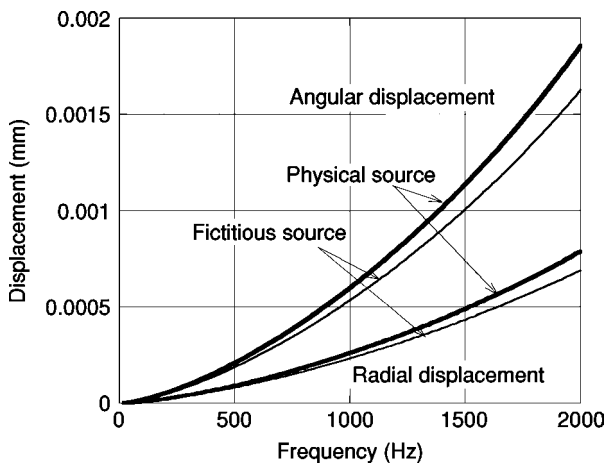


Figure 6. A comparison of radial (primarily attributable to P-waves) and angular (primarily attributable to S-waves) displacements for the physical and fictitious sources measured 100 m away from the 2D OVSs. The fictitious sources somewhat underestimate the amplitudes of the generated waves.

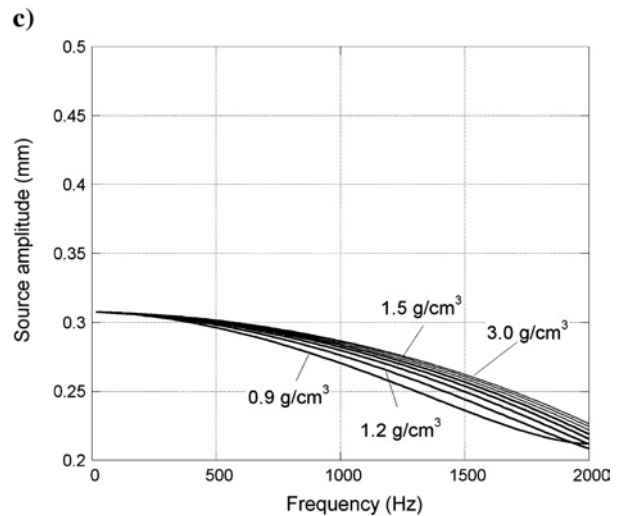
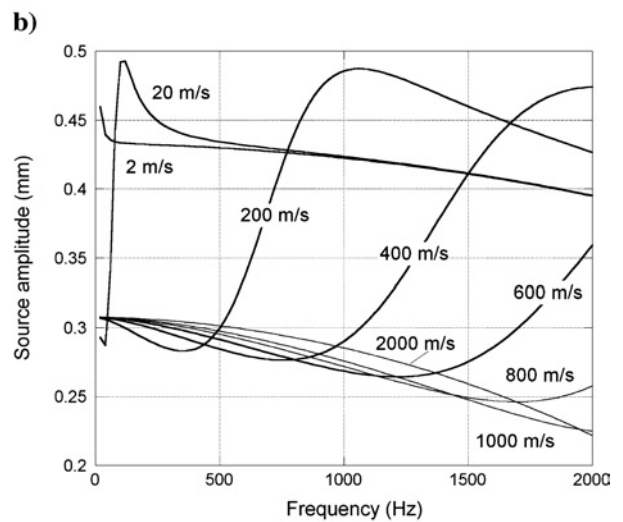
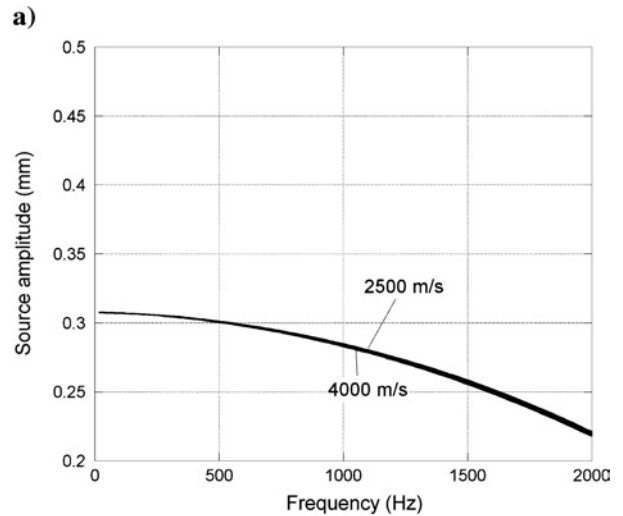


Figure 7. Parametric study of the 2D OVS displacement using the baseline properties shown in Table 1. For a practical range of material properties, an OVS shows some sensitivity to formation density and S-wave velocity but little sensitivity to P-wave velocity. (a) P-wave sensitivity; (b) S-wave sensitivity; (c) density sensitivity.

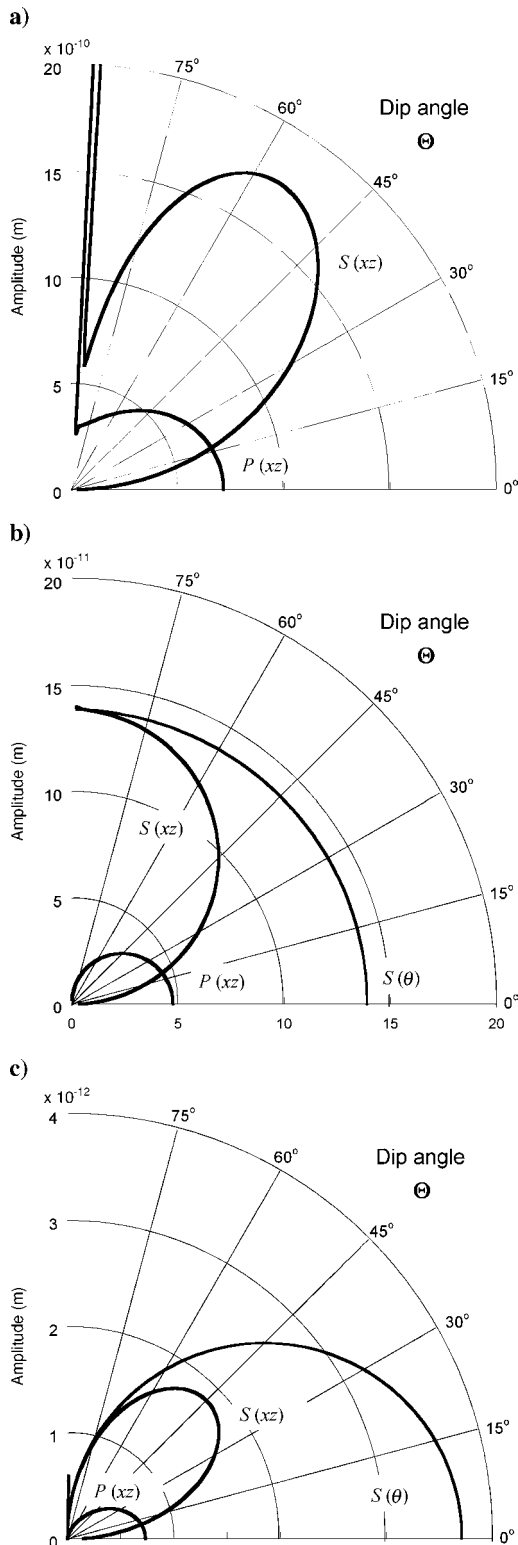


Figure 8. Radiation pattern of waves generated by OVSs of order (a)  $m = 0$  (monopole), (b)  $m = 1$  (dipole), and (c)  $m = 2$  (quadrupole). The values  $P(xz)$  and  $S(xz)$  indicate displacement components of P- and S-waves within the plane parallel to the borehole;  $S(\theta)$  indicates the S-wave amplitude normal to the borehole. The value  $P(xz)$  closely equals the P-wave amplitude, and  $S(xz)$  and  $S(\theta)$  are the SV- and SH-wave amplitudes, respectively.

maximum operational frequency of 400 Hz. For very small S-wave formation velocities, however, the weak (attenuated) resonance of the system shifts to lower frequencies, causing significant changes in the source amplitude. As the formation S-wave velocity approaches zero, the OVS source amplitude increases significantly for the entire frequency band.

### Radiation pattern of a 3D OVS

Using the discrete wavenumber method, the displacement wavefield generated by OVSs of different orders can be computed to study the radiation characteristics of the source. The following examples are given for the parameters in Table 1, with a frequency of 200 Hz and a source-receiver distance of 100 m. The point-volume source amplitude ( $V_0$ ) of all sources is given by equation 32, even for sources on the order of  $m \neq 1$ . Also, for the stability of the wavenumber integration, we assume small attenuation in the rock (seismic quality factor  $Q = 500$ ) and rather large attenuation in the fluid ( $Q = 100$ ). The large attenuation is used in the fluid to suppress the tube waves, and this has very small effect on the radiation pattern of the body waves.

The zero-order ( $m = 0$ ) OVS is a ring-shaped explosion source (monopole); the radiation patterns of the generated waves are very similar to those of a single-point volume source located on the borehole axis (e.g., Lee and Balch, 1982). Amplitudes of the displacement in a single radial plane are shown in Figure 8a as a function of the dip angle  $\Theta$  from the source plane. Because of the angular symmetry of the source around the borehole axis, SH-waves are not generated. From the figure we can see that this type of source generates P-waves [shown as  $P(xz)$  in the figure] that have a radiation pattern with a wide angular coverage in the vertical directions. The source also generates SV-waves [shown as  $S(xz)$ ] with significant amplitudes. However, the amplitude of the SV-waves diminishes to zero in the zero vertical-offset directions (horizontal directions), which is not desirable for crosswell measurements of waves. This type of source also generates large tube waves, as shown in the plot.

In contrast, the currently used OVS ( $m = 1$ ) generates significantly large SH-waves compared to P-waves, shown as  $S(\theta)$  and  $P(xz)$  in Figure 8b. The overall magnitude of the waves, however, is much smaller than the zero-mode source because dipole sources are less effective than monopole sources. The radiation pattern of the SH-waves is nearly spherical and lacks the nodal plane in the  $\Theta = 0$  direction, as seen for the  $m = 0$  case. This lack of an S-wave blind spot makes an OVS an ideal borehole source, particularly for crosshole surveys. Further, no significant amplitude of borehole-guided waves is seen near the borehole. The large SH-waves in the horizontal direction are also predicted by Dong (1994b) and observed in the field (e.g., Hardage, 1992).

For higher-order modes, the amplitudes of the waves generated by the vibrator become increasingly smaller. However, SH-waves are always generated by the sources, and their relative amplitudes compared to the P-waves are significantly large. Radiation patterns for modes greater than one maintain good coverage over a wide range of vertical offset angles except for the angles near borehole-parallel directions. An example for the second ( $m = 2$ ) mode is shown in Figure 8c.

### Borehole-guided waves

An OVS also generates guided waves along the borehole. To use an OVS for logging applications, it is important to suppress the borehole-guided waves for reliable S-wave measurements. Among conventional, nonrotating sources, multipole sources have been shown to be particularly effective in reducing guided-wave noises in S-wave measurements (Chen and Eriksen, 1991). This has a strong implication for the guided-wave generation by an OVS that is essentially a rotating multipole source.

For the  $m$ th-order OVS source, an infinite series of guided waves is generated that is characterized by the dispersion

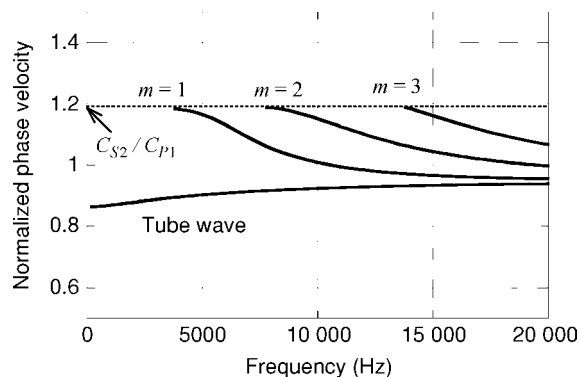


Figure 9. Dispersion of fundamental-mode, borehole-guided waves generated by  $m$ th-order OVSs. Velocities are normalized by the fluid P-wave velocity;  $m = 0$  corresponds to the tube waves. For higher-order sources ( $m > 0$ ), the guided waves have cutoff frequencies well above the frequencies used in the field.

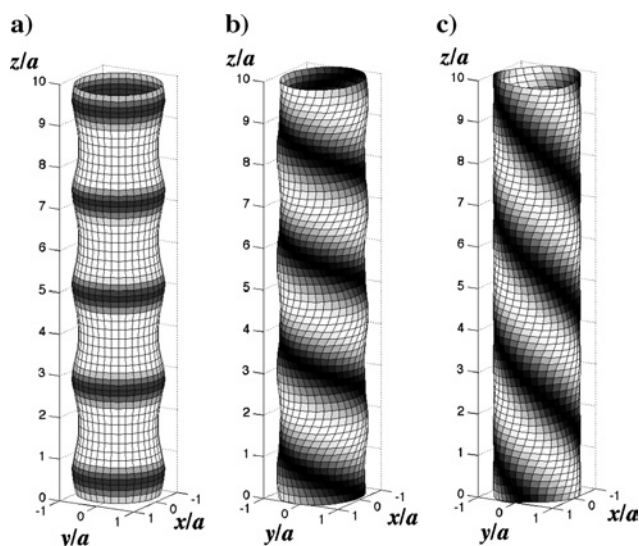


Figure 10. Borehole-wall mode shapes of borehole-guided waves (fundamental modes) for generalized OVSs of order (a)  $m = 0$ , (b)  $m = 1$ , and (c)  $m = 2$ . To compare the mode shapes of propagating guided waves, a high, single frequency of 15 kHz was selected. Light and dark colors indicate low and high fluid pressure on the wall. Because of the rotation of the source, the higher-order modes have a twisted mode shape.

equation

$$\det[\mathbf{M}_m(k_z, \omega)] = 0, \quad (37)$$

where  $\mathbf{M}_m$  is the matrix given by equation 33. Similar to the body waves, an OVS of order  $m$  can generate only the guided waves of order  $m$ . These equations are the dispersion equations of borehole-guided waves of arbitrary radial and circumferential orders. For the case  $m = 0$ , equation 37 becomes the dispersion equation for the borehole-guided waves studied by Biot (1952); the equation has an infinite number of solutions. For  $m = 0$ , the fundamental mode of the solutions is known as a tube wave which, for borehole fluids with P-wave velocity lower than the surrounding rock's S-wave velocity, exists at all frequencies and propagates at velocities less than the P-wave velocity of the borehole fluid. For  $m \geq 1$ , equation 37 also generates an infinite number of solutions for each  $m$ . However, these waves do not propagate (complex-valued solution) at low frequencies. As an example, the phase-velocity dispersion of the fundamental modes of order  $m = 0, 1, 2$ , and 3 is shown in Figure 9 (for the properties shown in Table 1).

A unique property of the orbital vibrator-generated, borehole-guided waves with higher circumferential orders ( $m \geq 1$ ) is that the mode shapes of the tube waves rotate around the borehole axis as the wave propagates along the borehole. Because of this, the mode shapes have a twisted appearance around the borehole axis (Figure 10). The dispersion characteristics of these guided waves, however, are the same as the guided waves generated by conventional sources (e.g., Paillet and White, 1982) because dispersion equation 37 is irrelevant to the source term.

An important consequence of the mode-selective property of an OVS is that, except for the  $m = 0$  case, body waves are generated below the cutoff frequency of the related guided waves. This should improve the quality of body-wave seismograms measured using an OVS by reducing the noise originated by borehole-guided waves. However, this may not be the case when the polar symmetry in the geometry of the borehole and the vibrator body is broken as a result of the heterogeneity in the surrounding rocks, a wash-out zone around the borehole, and the shifted center of the vibrator axis off the borehole axis; an imperfect mode selection generates tube waves. Although the effect of misalignment can be examined analytically (e.g., Nakagawa et al., 2003), the effect of heterogeneity must be examined using numerical simulations.

### CONCLUSIONS

In this article we develop both 2D and 3D semianalytical models for a fluid-coupled P- and S-wave source known as an OVS. A 2D OVS model is developed using physical source parameters following the technique developed by Reynolds and Cole. The 3D model is developed by envisioning the source as single and distributed arrays of point sources, an extension of Dong's model.

From the model derivation, we can see that the fundamental mechanism of S-wave generation by an OVS can be modeled by converting of P-waves into S-waves on the borehole wall. Although an OVS is a fluid-coupled source, the 2D model indicates that the source motion itself is insensitive to P-wave acoustic impedance of the formation yet is somewhat

dependent on the S-wave impedance. This can be explained by the dipole (or multipole) nature of the source because the net volume change within the borehole fluid is zero — the same mechanism utilized by multipole S-wave logging tools. The 2D source model is also useful for examining the relationship between source parameters and amplitudes of generated waves. However, the relationships may not be accurate quantitatively because the model assumes an infinite source length.

Instead of solving a physical 3D source problem that can be quite complicated mathematically, we use a relatively simple point-source array representation of an OVS source. Our 3D source predicts very uniform, spherical radiation patterns of SH-waves generated by an OVS, which suggests the source can be used for wide-angle crosshole, vertical seismic profiling, and single-hole seismic measurements. Further, the theory indicates that, under ideal conditions, an OVS should generate no borehole-guided waves at frequencies used in the field. This is not usually the case for real measurements where an OVS is located off the borehole axis and heterogeneities are present in the formation surrounding the borehole. The effect of heterogeneity and the background formation structures and anisotropy are difficult to examine using our semianalytical model, and this needs to be studied numerically. However, our model provides clear physical insight into the mechanism of wave generation and is a tool to quickly estimate the amplitude and radiation of waves generated by an OVS.

## ACKNOWLEDGMENTS

This research has been supported by the Office of Science, Office of Basic Energy Sciences, Division of Chemical Sciences of the U. S. Department of Energy under contract DE-AC76SF00098 and by the Assistant Secretary for Fossil Energy, Office of Oil and Natural Gas, National Energy Technology Laboratory, of the U. S. Department of Energy under contract DE-AC03-76SF00098. The authors thank Steven R. Pride (Lawrence Berkeley National Laboratory) for the discussion regarding the validity of the acoustic approximation used in the source modeling.

## APPENDIX A

### JUSTIFICATION FOR USE OF THE ACOUSTIC-WAVE EQUATION IN BOREHOLE FLUIDS

The Navier-Stokes equation for wave propagation within a borehole fluid is

$$\rho_f \left( \frac{\partial}{\partial t} \mathbf{v} + \mathbf{v} \cdot \nabla \mathbf{v} \right) = \mu_f \nabla^2 \mathbf{v} - \nabla p + (\mu_f/3 + \lambda_f) \nabla (\nabla \cdot \mathbf{v}), \quad (\text{A-1})$$

where  $\rho_f$  is the fluid density and where  $\mu_f$  and  $\lambda_f$  are the shear and bulk viscosity. By taking the divergence and time derivation of equation A-1 and also from the constitutive relationship

$$\nabla \cdot \mathbf{v} = -\frac{1}{K_f} \frac{\partial p}{\partial t}, \quad (\text{A-2})$$

we obtain

$$\begin{aligned} & \rho_f \frac{\partial^2}{\partial t^2} (\nabla \cdot \mathbf{v}) + \rho_f \frac{\partial}{\partial t} \nabla \cdot (\mathbf{v} \cdot \nabla \mathbf{v}) \\ & = K_f \nabla^2 (\nabla \cdot \mathbf{v}) + (4\mu_f/3 + \lambda_f) \frac{\partial}{\partial t} \nabla^2 (\nabla \cdot \mathbf{v}). \end{aligned} \quad (\text{A-3})$$

Here,  $K_f$  is the fluid bulk modulus. We first compare the two terms on the right-hand side of the equation. By replacing the time derivative by  $-i\omega t$ , the relative magnitude of the second term with respect to the first term is

$$\begin{aligned} \frac{(4\mu_f/3 + \lambda_f)\omega}{K_f} &= \frac{4/3 \cdot 10^{-3} + 2.8 \cdot 10^{-3}}{2.25 \times 10^9} \\ &\times \omega = (1.15 \times 10^{-11}) \times f. \end{aligned} \quad (\text{A-4})$$

Therefore, the viscosity term can be neglected for all frequencies of interest for our problems (up to several kilohertz).

Next, we evaluate the relative magnitude of the second term (nonlinear convection term) of the left-hand side of the equation against the first term. Here, as an approximation, we replace the nabla operator  $\nabla$  by the inverse of a characteristic length, e.g., the source radius. Using the approximate source displacement  $u = 0.5$  mm from the 2D analysis yields

$$\left| \frac{\rho_f \omega \nabla \cdot (\mathbf{v} \cdot \nabla \mathbf{v})}{\rho_f \omega^2 (\nabla \cdot \mathbf{v})} \right| \sim \frac{u}{a} = \frac{0.5 \times 10^{-3}}{50 \times 10^{-3}} = 0.01 \ll 1. \quad (\text{A-5})$$

Therefore, the nonlinear term can be neglected.

Returning to the original equation without the nonlinear and viscosity terms, by applying the divergence to the equation and using the constitutive equation,

$$\frac{\rho_f}{K_f} \frac{\partial^2}{\partial t^2} p = \nabla^2 p. \quad (\text{A-6})$$

This is the acoustic-wave equation.

## APPENDIX B

### PARTIAL-WAVE EXPANSION OF SOLUTIONS IN CYLINDRICAL COORDINATES

The wavefield outside a borehole can be computed from three scalar displacement potentials  $\Phi_p$ ,  $\Phi_{SH}$ , and  $\Phi_{SV}$ . The components of displacement are computed using these potentials as (e.g., Kurkjian and Chang, 1986)

$$\mathbf{u} = \nabla \Phi_p + \nabla \times (\hat{\mathbf{z}} \Phi_{SH}) + \nabla \times \nabla \times (\hat{\mathbf{z}} \Phi_{SV}). \quad (\text{B-1})$$

In cylindrical coordinates, the components of the displacement are

$$u_r = \frac{\partial \Phi_p}{\partial r} + \frac{1}{r} \frac{\partial \Phi_{SH}}{\partial \phi} + \frac{\partial^2 \Phi_{SV}}{\partial r \partial z}, \quad (\text{B-2})$$

$$u_\phi = \frac{1}{r} \frac{\partial \Phi_p}{\partial \phi} - \frac{\partial \Phi_{SH}}{\partial r} + \frac{1}{r} \frac{\partial^2 \Phi_{SV}}{\partial \phi \partial z}, \quad (\text{B-3})$$

$$u_z = \frac{\partial \Phi_p}{\partial z} - \frac{\partial^2 \Phi_{SV}}{\partial r^2} - \frac{1}{r} \frac{\partial \Phi_{SV}}{\partial r} - \frac{1}{r^2} \frac{\partial^2 \Phi_{SV}}{\partial \phi^2}. \quad (\text{B-4})$$

For the acoustic fluid within a borehole, only the first term in equation B-1 is used, i.e.,  $\mathbf{u} = \nabla \Phi_p$ . For 2D problems, the

third term is not used. The displacement potentials individually satisfy Helmholtz equations and can be expressed in series form as

$$\Phi_P^{(1)} = \sum_{n=-\infty}^{\infty} A_n^P(k_z, \omega) J_n(k_r^{P1} r) e^{i(n\phi + k_z z - \omega t)}, \quad (\text{B-5})$$

$$\Phi_P^{(2)} = \sum_{n=-\infty}^{\infty} B_n^P(k_z, \omega) H_n^{(1)}(k_r^{P2} r) e^{i(n\phi + k_z z - \omega t)}, \quad (\text{B-6})$$

$$\Phi_{SH}^{(2)} = \sum_{n=-\infty}^{\infty} B_n^{SH}(k_z, \omega) H_n^{(1)}(k_r^{S2} r) e^{i(n\phi + k_z z - \omega t)}, \quad (\text{B-7})$$

$$\Phi_{SV}^{(2)} = \sum_{n=-\infty}^{\infty} a \cdot B_n^{SV}(k_z, \omega) H_n^{(1)}(k_r^{S2} r) e^{i(n\phi + k_z z - \omega t)} \quad (\text{B-8})$$

for 3D problems. The radius of the borehole  $a$  is included in equation B-8 to match the dimension of the coefficients. The superscripts 1 and 2 on the potentials denote inside and outside the borehole, respectively, which should not be confused with the superscripts on the Bessel (Hankel) functions. Also, the superscripts  $P1$ ,  $P2$ , and  $S2$  indicate P-waves inside and outside the borehole and the S-wave outside the borehole. The values  $k_r^{P1}$ ,  $k_r^{P2}$ , and  $k_r^{S2}$  are the radial components of the wavenumbers. Since the wavefield within the borehole is regular and the field outside the borehole is unbounded, Bessel functions of the first kind and Hankel functions of the first kind are used for inside and outside the borehole, respectively.

For the 2D problem with the physical source, equations (B5–B7) become

$$\Phi_P^{(1)} = \sum_{n=-\infty}^{\infty} \left[ A_n^{P+}(\omega) H_n^{(1)}(k_{P1} r) + A_n^{P-}(\omega) H_n^{(2)}(k_{P1} r) \right] \times e^{i(n\phi - \omega t)}, \quad (\text{B-9})$$

$$\Phi_P^{(2)} = \sum_{n=-\infty}^{\infty} B_n^P(k_z, \omega) H_n^{(1)}(k_{P2} r) e^{i(n\phi - \omega t)}, \quad (\text{B-10})$$

$$\Phi_{SH}^{(2)} = \sum_{n=-\infty}^{\infty} B_n^{SH}(k_z, \omega) H_n^{(1)}(k_{S2} r) e^{i(n\phi - \omega t)}, \quad (\text{B-11})$$

where  $k_{P1} \equiv \omega/c_{P1}$ ,  $k_{P2} \equiv \omega/c_{P2}$ , and  $k_{S2} \equiv \omega/c_{S2}$ . In this case, since the wavefield within the borehole fluid is bounded by the borehole wall as well as the source surface, both kinds of Hankel functions are used in equation B-9.

The stress components are obtained by first computing strain components from equations B-2, B-3, and B-4 and then applying Hooke's law to the strains.

## REFERENCES

- Biot, M. A., 1952, Propagation of elastic waves in a cylindrical bore containing a fluid: *Journal of Applied Physics*, **23**, 997–1009.
- Chen, S. T., and E. A. Eriksen, 1991, Compressional and shear-wave logging in open and cased holes using multipole tool: *Geophysics*, **56**, 550–557.
- Cole, J. H., 1997, The orbital vibrator, a new tool for characterizing interwell reservoir space: *The Leading Edge*, **16**, 281–283.
- Daley, T. M., and D. Cox, 2001, Orbital vibrator seismic source for simultaneous P- and S-wave crosswell acquisition: *Geophysics*, **66**, 1471–1480.
- Dong, W., 1994a, Elastic wave radiation from borehole seismic sources in anisotropic media: Ph.D dissertation, Massachusetts Institute of Technology.
- , 1994b, A mathematical model for the downhole orbital vibrator source: 64th Annual International Meeting, SEG, Expanded Abstracts, 90–93.
- Dong, W., M. Bouchon, and M. N. Toksoz, 1995, Borehole seismic-source radiation in layered isotropic and anisotropic media: Boundary element modeling: *Geophysics*, **60**, 735–747.
- Hardage, B. A., 1992, *Crosswell seismology and reverse VSP*: Geophysical Press.
- Kurkjian, A. L., and S. K. Chang, 1986, Acoustic multipole sources in fluid-filled boreholes: *Geophysics*, **51**, 148–163.
- Lee, M. W., and A. H. Balch, 1982, Theoretical seismic wave radiation from a fluid-filled borehole: *Geophysics*, **47**, 1308–1314.
- Liu, E., S. Crampin, and J. H. Queen, 1991, Fracture detection using crosshole surveys and reverse vertical seismic profiles at the Conoco Borehole Test Facility, Oklahoma: *Geophysical Journal International*, **107**, 449–463.
- Liu, E., J. H. Queen, and V. D. Cox, 2000, Anisotropy and attenuation of crosshole channel waves from the Antrim Shale gas play, Michigan basin: *Journal of Applied Geophysics*, **44**, 47–61.
- Nakagawa, S., T. M. Daley, and E. L. Majer, 2003, Waves generated by borehole orbital vibrator source: 73rd Annual International Meeting, SEG, Expanded Abstracts, 2247–2250.
- Novascone, S. R., M. J. Anderson, D. M. Weinberg, and J. H. Cole, 2002, Driving point impedance and physical property logging: 72nd Annual International Meeting, SEG, Expanded Abstracts, 2467–2470.
- Paillet, F. L., and J. E. White, 1982, Acoustic modes of propagation in the borehole and their relationship to rock properties: *Geophysics*, **47**, 1215–1228.
- Reynolds, R. R., and J. H. Cole, 2002, Propagation from a fluid-encased vibrator in an elastic continuum: 22nd Southeastern Conference on Experimental and Applied Mechanics, Proceedings, **525–534**.
- Van Schaack, M., J. M. Harris, J. W. Rector III, and S. K. Lazaratos, 1995, High-resolution crosswell imaging of a West Texas carbonate reservoir: Part 2—Wavefield modeling and analysis: *Geophysics*, **60**, 682–691.